

A novel phosphorus diffusion process for front-side P–N junction fabrication in PERC solar cells



Yixuan Huang^a, Longqing Jiang^a, Long Yan^a, Yang Yang^b, Rulong Chen^b, Hui Cui^c, Geng Su^c, Honggang Zhang^c, Baoju Yang^c, Juan Hong^{a,*}

^a College of Mechanical Engineering, Yancheng Institute of Technology, Yancheng, Jiangsu, 224051, PR China

^b Jiangsu Runergy Yueda PV Technology Co., Ltd, Yancheng, Jiangsu, 224000, PR China

^c Yancheng Gaoce New Energy Technology Co.,Ltd, Yancheng, 224700, PR China

ARTICLE INFO

Keywords:

PERC solar cells
Phosphorus diffusion
P-n junction
Photovoltaic conversion efficiency

ABSTRACT

P–N junction technology underlies photovoltaic conversion in passive emitter and rear cell (PERC) solar cells. Although the front-side phosphorus diffusion method for creating P-type PERC cells is well researched, avenues for innovation persist. We introduce a P–N junction fabrication technique for PERC solar cells via precisely controlling the surface doping concentration and junction depth. Through pressure modulation and carefully selected annealing duration at a defined temperature, the technique yields a P–N junction with a surface doping concentration of $2.37 \times 10^{20} \text{ cm}^{-3}$ and a junction depth of 0.29 μm on the front surface of PERC cells. Compared to conventional diffusion processes, our approach results in an average increase of 1.3 mV in open-circuit voltage, 20 mA in short-circuit current, and an efficiency gain of 0.05 %. The maximum efficiency achieved is 23.68 %, representing an improvement of 0.16 %.

1. Introduction

In recent years, the proportion of photovoltaic power generation within the overall electricity supply system has been steadily increasing. Crystalline silicon solar cells, as a central component of photovoltaic power generation, have gained increasing prominence in their significance. Addressing issues such as global warming and the growing scarcity of energy resources has become a global consensus, leading to the development of clean energy sources. Solar energy, being a renewable resource, offers advantages in terms of cleanliness, safety, and abundant availability. Consequently, solar photovoltaic technology has been widely promoted and adopted [1–3]. Within this field, the passive emitter and rear cell (PERC) technology for crystalline silicon solar cells has emerged as the mainstream approach for enhancing solar cell efficiency [4–7]. Building upon this foundation, the P–N junction fabrication technique through phosphorus diffusion has progressively matured and achieved industrial-scale production. Furthermore, due to its advantages in ease of production line upgrade and compatibility, it is gradually becoming the new mainstream for next-generation products.

The photovoltaic conversion efficiency of solar cells is primarily influenced by the open-circuit voltage, fill factor, short-circuit current,

series resistance, and shunt resistance [8]. The process of fabricating the P–N junction through diffusion plays a crucial role in enhancing the photovoltaic conversion efficiency of solar cells, particularly in terms of the open-circuit voltage, fill factor, and short-circuit current. Through software simulation and analysis [9–11], it has been determined that a lower surface concentration and deeper junction depth during the P–N junction fabrication process can significantly improve the photovoltaic conversion efficiency of solar cells. Temperature notably affects junction depth and surface concentration, and thus, by refining the diffusion process temperature, it is possible to fabricate P–N junctions with lower surface phosphorus concentration and deeper junction depth [12–14], thereby further enhancing the photovoltaic conversion efficiency.

Currently, the conventional production process of crystalline silicon solar cells is evolving toward higher sheet resistance. High sheet resistance emitter solar cells, owing to their excellent short-wavelength spectral response and carrier recombination properties, represent an effective approach for achieving high-efficiency solar cells. However, the increase in emitter sheet resistance poses challenges in controlling diffusion uniformity, thereby affecting the stability of solar cell processes. Therefore, optimizing diffusion process parameters plays a crucial role in enhancing sheet resistance uniformity and improving the

* Corresponding author. Hope Avenue Road 1, 224051, Yancheng, Jiangsu province, PR China.

E-mail address: jameshong@ycit.cn (J. Hong).

Table 1

Main parameters of simulated PERC solar cells.

Parameter	Input data
Background dopant species	Boron
Profile dopant species	Phosphorus
Background dopant concentration (cm^{-3})	1×10^{16}
Background thickness (μm)	183
Background resistivity (Ωcm)	0.8
Doping function	ERFC

stability of solar cell processes [15,16]. Li et al. investigated the effect of boron diffusion characteristics on solar cell performance and found that increasing the depth of the P–N junction could lead to higher photovoltaic conversion efficiency. Specifically, when the dopant concentration was $2 \times 10^{19} \text{ cm}^{-3}$, the photovoltaic conversion efficiency could be improved to 21.8 % [17]. Long et al. studied the influence of low-pressure diffusion processes on large-scale silicon wafers and observed that employing low-pressure diffusion processes improved the uniformity within the furnace and at the furnace mouth [18]. Zhang et al. optimized the phosphorus diffusion process and discovered that increasing the surface phosphorus doping concentration could enhance the open-circuit voltage and subsequently improve the cell's conversion efficiency. Specifically, when the surface phosphorus doping concentration was $2.8 \times 10^{20} \text{ cm}^{-3}$, the photovoltaic conversion efficiency could be increased by 0.2 % [19]. Liu et al. investigated the influence of emitter surface doping concentration on solar cell performance and found that silicon wafers with low surface doping concentration and deep junction depth exhibited higher photovoltaic conversion efficiency. Notably, when the surface doping concentration was $3.12 \times 10^{20} \text{ cm}^{-3}$, the photovoltaic conversion efficiency could be increased by 0.26 % [20].

The aforementioned studies have all optimized diffusion processes and improved doping concentrations to further enhance the photovoltaic conversion efficiency of solar cells. Building on the theoretical analysis provided earlier, this study explores a novel diffusion process suitable for P-type PERC crystalline silicon solar cells. This involves adjusting the gas pressure during the push-in and deposition steps, extending the annealing time, and ultimately fabricating a P–N junction with a low surface phosphorus concentration, high junction depth, and improved uniformity. Additionally, by carefully controlling the temperature in the constant-temperature region, solar cell wafers with high sheet resistance are prepared. Through these comprehensive approaches, we achieve solar cell wafers with both high photovoltaic conversion efficiency and superior uniformity in sheet resistance.

2. Simulation and experiments

2.1. Simulation

To examine the influence of front surface phosphorus diffusion concentration on PERC cell efficiency, this study utilized EDNA2 to compute the surface recombination velocity of the emitter and PC1D to determine the sheet resistance and junction depth at the emitter surface. Additionally, we conducted an analysis of the relationship between the front surface phosphorus doping concentration and the emitter surface saturation current and junction depth [21–24]. Table 1 provides all the simulated input parameters for the selective PERC structure at the front surface. The cell thickness of this structure is 183 μm , with a resistivity of 0.8 Ωcm .

Using the aforementioned simulated parameters, we calculated the relationship between the surface recombination velocity, saturation current, junction depth, and surface doping concentration [25]. The simulation results are depicted in Fig. 1. As shown in Fig. 1(a), it is evident that as the surface doping concentration increases, the junction depth gradually becomes shallower. Furthermore, with the rise in surface doping concentration, the emitter saturation current increases, and concurrently, the surface recombination velocity also intensifies. These factors collectively contribute to a decrease in the photovoltaic conversion efficiency of the solar cell, as illustrated in Fig. 1(b). This decline primarily results from the expansion of the electric field into deeper layers as the surface doping concentration increases, leading to a reduction in junction depth and an increase in the loss of photo-generated carriers.

Based on the comprehensive analysis conducted, it becomes evident that the phosphorous doping concentration on the emitter surface significantly influences the conversion efficiency of PERC solar cells. Striking a delicate balance between the surface phosphorous doping concentration and junction depth is crucial. Remarkably, when the surface phosphorous doping concentration falls within the range of $2.2 \times 10^{20} \text{ cm}^{-3}$ to $3.1 \times 10^{20} \text{ cm}^{-3}$, the junction depth stabilizes at 0.15 μm . Utilizing lower surface doping concentrations and deeper junction depths effectively suppresses surface recombination rates, enhances the utilization of short wavelengths, and reduces emitter recombination currents. These improvements ultimately prove advantageous in augmenting the conversion efficiency of PERC solar cells.

2.2. Experimental

A total of 1200 monocrystalline silicon wafers, provided by Qujing Longji Limited Company, were selected for this study. Each wafer

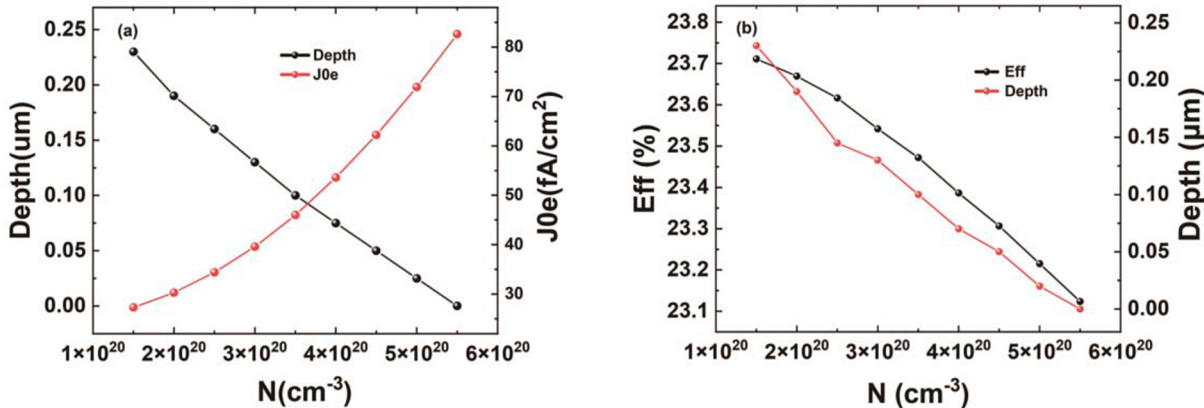


Fig. 1. The simulated data presented in Fig. (a) illustrate the relationship between the surface doping concentration and the doping depth as well as the surface recombination current density, J_{0e} . Meanwhile, Fig. (b) exhibits the correlation between the surface doping concentration and the doping depth, along with the photovoltaic conversion efficiency.

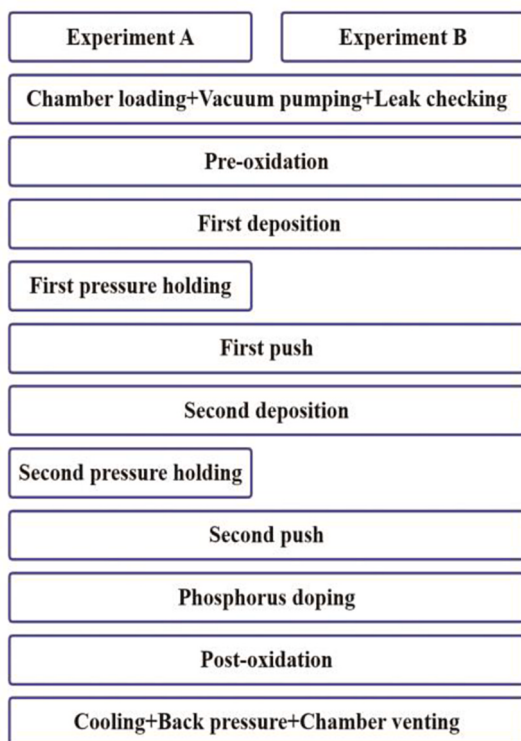


Fig. 2. Diffusion process flow charts for Group A and Group B experiments.

possesses a thickness of $155 \pm 10 \mu\text{m}$ and dimensions measuring $182 \text{ mm} \times 183.75 \text{ mm}$. These wafers underwent a sorting process employing a sorting machine, resulting in a resistivity range of $0.6\text{--}0.9 \Omega\cdot\text{cm}$.

Following the sorting process, the silicon wafers were subjected to an identical texturing process and subsequently divided into two equal groups: Group A (referred to as "A samples") and Group B (referred to as

"B samples"), each comprising 600 wafers. The A samples were processed using a novel diffusion method to create p-n junctions, aiming for a high sheet resistance of approximately $130 \Omega/\square$. In contrast, the B samples were prepared using a conventional diffusion process, targeting a typical sheet resistance of approximately $120 \Omega/\square$. To ensure consistency, both groups of samples were placed in the same diffusion furnace for experimentation. The middle region of the furnace, known for its stable sheet resistance and superior uniformity compared to the inlet and outlet regions, was selected as the optimal location [26,27]. Moreover, using a single furnace eliminated potential variations that could arise from using multiple furnaces. Following the diffusion process, both groups of samples underwent identical subsequent processes, including etching, oxidation, coating, and printing sintering. Subsequently, the electrical performance parameters of the resulting solar cells were characterized through testing, referred to as Group A cells and Group B cells in subsequent analysis.

The novel diffusion process introduces two key modifications compared to the conventional diffusion process [28–30]. First, it incorporates an additional 190 s pressurization step after the deposition phase. This step enhances the stability of the gas pressure within the furnace tube, preparing it for the subsequent phosphorus source step and improving the uniformity of the diffusion sheet resistance. Second, the annealing step is extended by an additional 240 s, building upon the previous annealing time. This extension enhances the effectiveness of dopant incorporation, resulting in a lower surface phosphorus concentration and deeper p-n junctions. Consequently, a noticeable increase in the open-circuit voltage is anticipated, along with an expected improvement in the photovoltaic conversion efficiency. The pressurization step and the extended annealing time lead to a lower sheet resistance compared to the conventional diffusion process. To compensate for this, temperature compensation will be employed to adjust the temperature-dependent sheet resistance to its normal range. Lowering the temperature reduces thermal damage and aids in enhancing the open-circuit voltage. Overall, the novel diffusion process increases the total duration by 430 s, but its effect on the entire process flow is minimal. Fig. 2 illustrates the schematic representation of the

Table 2

The data for the square resistance of samples A and B after diffusion are as follows.

Group	Parameter	(20 cells)	Furnace mouth	Inside the furnace	Furnace tail	Average
A	Sheet resistance (Ω/\square)	± 0.1	124	129	132	126
	Uniformity (%)	± 0.01	6.00	5.54	5.74	8.84
B	Sheet resistance (Ω/\square)	± 0.1	120	121	120	122
	Uniformity (%)	± 0.01	4.37	5.70 %	5.04	7.61

The data were measured at China Jiangsu Runergy Yueda PV Technology Co., Ltd.

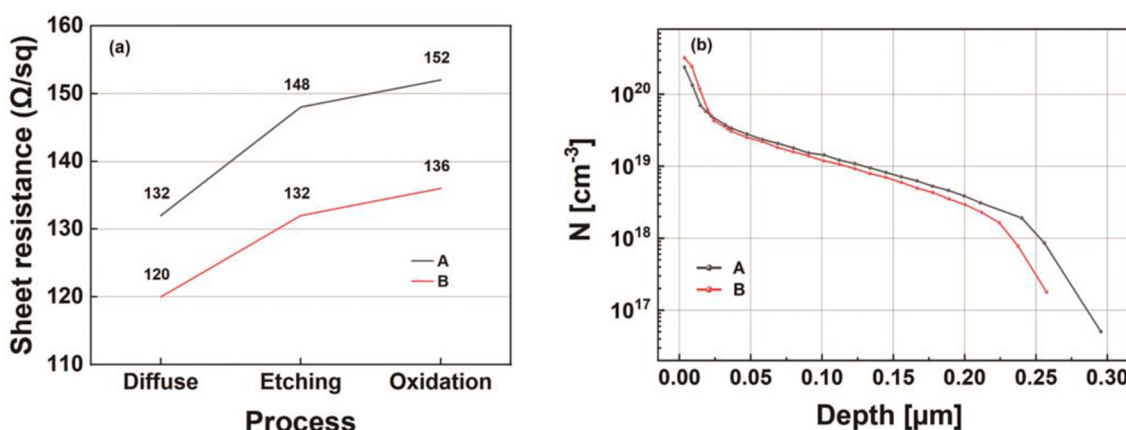


Fig. 3. The monitoring data for samples in Group A and Group B are presented as follows: (a) data showing the increase in sheet resistance after diffusion, alkaline etching, and oxidation; (b) data characterizing the effective carrier lifetime (ECV) after diffusion.

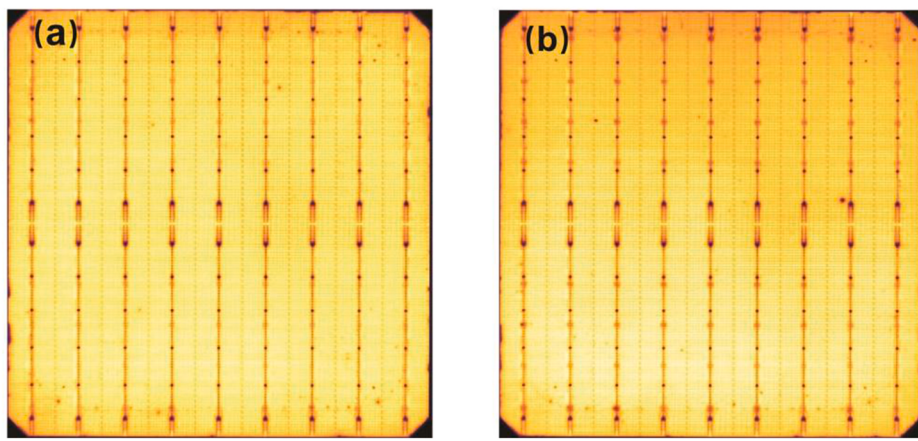


Fig. 4. PL test characterization data: (a) PL brightness diagram of group A samples; (b) PL brightness chart of group B samples.

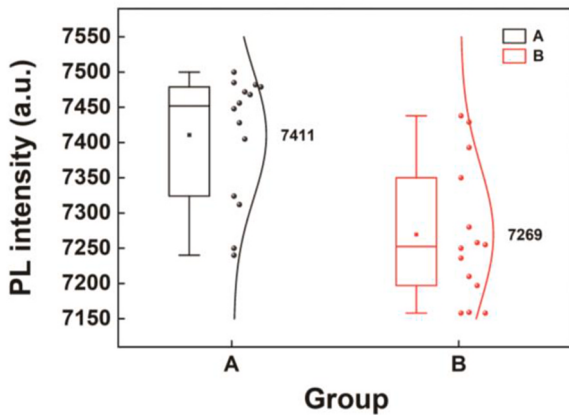


Fig. 5. PL brightness characterization data of group a and group b samples.

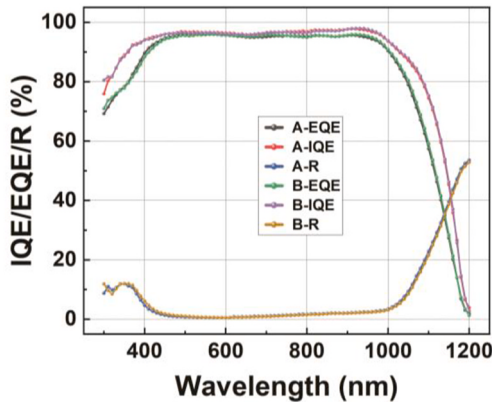


Fig. 6. Characterization data of EQE, IQE and r of group A and group b samples.

different diffusion processes employed for the two groups of silicon wafers.

2.3. Experimental apparatus

In this study, the assessment of solar cell luminance under illumination, as well as the determination of carrier density and lifetime within the corresponding region, was conducted using the LIS-R3 measurement system from the Australian company BT Imaging. To

Table 3
Characterization data of EQE, IQE of Group A and Group B samples.

Group	EQE mA/cm ²	IQE mA/cm ²	EQE (mA/cm ²)		
			300–600 nm	610–900 nm	910–1200 nm
A	40.63	42.06	12.68	19.25	8.74
B	40.54	42.02	12.59	19.22	8.69
(20 cells)	± 0.01	± 0.01	± 0.01	± 0.01	± 0.01

The data were measured at China Jiangsu Runergy Yueda PV Technology Co., Ltd.

accurately determine the spectral response EQE and IQE of the solar cells, the MNPVQE-300 quantum efficiency (QE) tester from the American company Mennekes was employed. The square resistance of the diffused silicon wafers was measured utilizing a four-dimensional cube resistance tester from the United States. The depth of the p-n junction on the surface of laser-doped silicon wafers, hereafter referred to as the “junction depth,” and the surface phosphorus diffusion concentration of the diffusion layer were determined using the CVP21 apparatus from the German company WEP. Additionally, the square resistance and contact resistance of the finished cells were measured with the transmission line method (TLM) tester from the German company PV-tools. Last, the conversion efficiency of the finished cells was measured using the high-precision I-V measurement system from the German company Halm.

3. Results and discussion

3.1. Square resistance analysis

Two sets of samples, denoted as A and B, each comprising two pieces, were extracted from the inlet, middle, and outlet positions of the furnace. The square resistance of the diffused samples was measured. Subsequently, both sets underwent standardized procedures to produce finished cells, and the electrical performance parameters of these cells were collected, including the measurement of contact resistance values.

Following the diffusion process, temperature compensation was applied to the A and B samples to maintain the square resistance within the furnace tube at approximately $120 \Omega/\square$ and $130 \Omega/\square$ [31]. Actual measurements were conducted at 25 points using a four-dimensional cube resistance tester, and average values were derived. The A samples exhibited a square resistance of $132 \Omega/\square$ in the middle of the furnace with a uniformity of 7.23 %, while the B samples showed a square resistance of $120 \Omega/\square$ in the same region with a uniformity of 6.325 %. Both sets met the expected square resistance control values, albeit with slightly lower uniformity in the A samples compared to the B

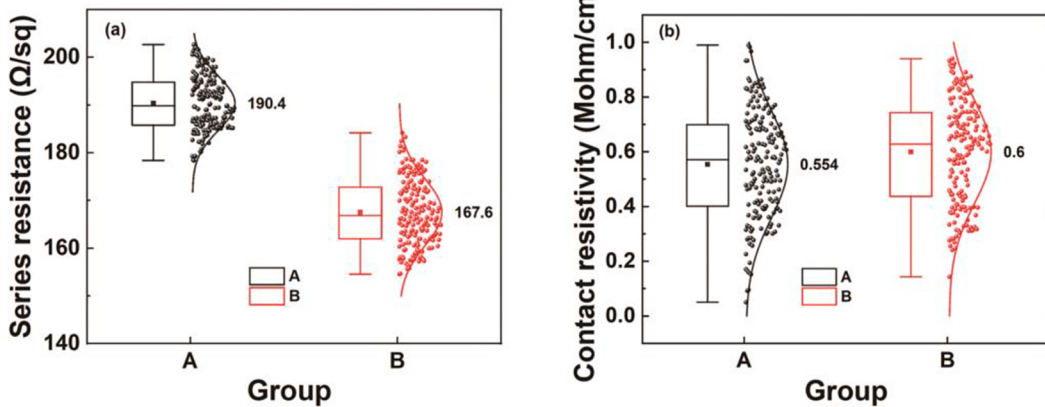


Fig. 7. TLM characterization data: (a) series resistance of group a and group b; (b) contact resistivity of group A and group B.

Table 4
Electrical performance parameters of group A and group B finished solar cells.

Group	Eff (%)	Voc (mV)	Isc (A)	FF (%)	Rs ($\text{m}\Omega$)	Rsh (Ω)	Yield (%)
A	23.53	688.4	13.81	82.40	0.91	788	96.50
B	23.48	687.1	13.79	82.48	0.87	632	94.28
(600 cells)	± 0.01	± 0.1	± 0.01	± 0.01	± 0.01	± 0.01	± 0.01

The data were measured at China Jiangsu Runergy Yueda PV Technology Co., Ltd.

samples. This variation in uniformity can be attributed to the inherent challenge of achieving uniformity in the production of high-resistance solar cells. However, it is noteworthy that this difference is minimal and exerts a limited effect on cell efficiency, as indicated in Table 2.

The production of emitter electrodes with exceptional uniformity in high-resistance cells not only reduces surface recombination and enhances the open-circuit voltage but also significantly improves the spectral response of short wavelengths, leading to an increase in the short-circuit current and an improvement in the photoelectric conversion efficiency of the cells.

3.2. Electrochemical voltage characterization testing

After the diffusion process, two solar samples were selected from each group for sheet resistance monitoring. This monitoring involved tracking the increase in sheet resistance following diffusion, alkaline etching, and oxidation, as well as checking for any process anomalies. The results are presented in Fig. 3(a). Notably, the sheet resistance monitoring for both experimental groups after diffusion remained within the normal range, indicating the absence of anomalies. Analyzing the data in Fig. 3(a) reveals that the Group A samples exhibited a $16 \Omega/\square$ increase in sheet resistance after alkaline etching, while the Group B samples demonstrated a $12 \Omega/\square$ increase. This suggests that high-resistance solar cells experienced a more substantial increase in sheet resistance following alkaline etching. However, the increase in sheet resistance after oxidation remained consistent at $4 \Omega/\square$ for both groups, showing no significant differences.

Subsequent to alkaline etching, two monitoring solar cells were selected to measure the electrochemical voltage (ECV) using the ECV electrochemical capacitance voltage method. This allowed for the determination of the phosphorus doping concentration and its depth distribution within the silicon wafers. The results are depicted in Fig. 3(b). From Fig. 3(b), it is evident that Group A exhibited a lower surface concentration and a deeper junction depth, aligning with the initial expectations. Extending the annealing time indeed led to a deeper p-n

junction, confirming the anticipated result.

The lower surface phosphorus doping concentration contributes to reduced surface recombination and enhanced minority carrier lifetime [32,33]. Simultaneously, the increased junction depth reduces contact resistivity, both of which confer advantages in terms of open-circuit voltage and short-circuit current.

3.3. PL characterization analysis

Following the completion of printing and sintering, 14 samples were randomly selected from both Group A and Group B for subsequent testing and characterization. Initially, the R3 device was employed for photoluminescence (PL) characterization analysis. This involved observing the imaging of the entire solar cell under uniform illumination from a light source. The intensity of localized emission in the images is determined by the carrier density and lifetime of the corresponding region [34], with higher emission indicating stronger pixel values. The PL characterization results for Group A and Group B are presented in Fig. 4 (a) and (b), respectively. It is evident that the luminescence brightness of Group A significantly surpasses that of Group B.

Fig. 5 offers a comparative analysis of the brightness values for Group A and Group B. The brightness value for Group A is recorded as 7411, whereas that for Group B is 7269. The 142-unit difference underscores the superior carrier density and lifetime exhibited by Group A. This observation finds further support in subsequent analysis of the electrical performance, notably reflected in the advantageous open-circuit voltage.

3.4. QE characterization analysis

Subsequently, the extracted samples underwent quantum efficiency testing, which involved measuring the solar cell's capability to convert incident photons of varying wavelengths into photocurrent output [35–37], as illustrated in Fig. 6. Analysis of both the EQE and current loss data, as presented in Table 3, reveals that the Group A specimens exhibit an advantage in the short wavelength range of 300–600 nm, outperforming the Group B specimens by 0.09 mA/cm^2 . This indicates that the positive short-wavelength spectral response of Group A is superior, enhancing the carrier recombination characteristics. This improvement can be primarily attributed to the pronounced advantages conferred by the high-resistance diffusion process employed.

3.5. TLM characterization analysis

One representative cell from each group, as selected from the PL measurements, underwent further characterization using TLM testing [38]. The TLM analysis revealed that the new diffusion process resulted

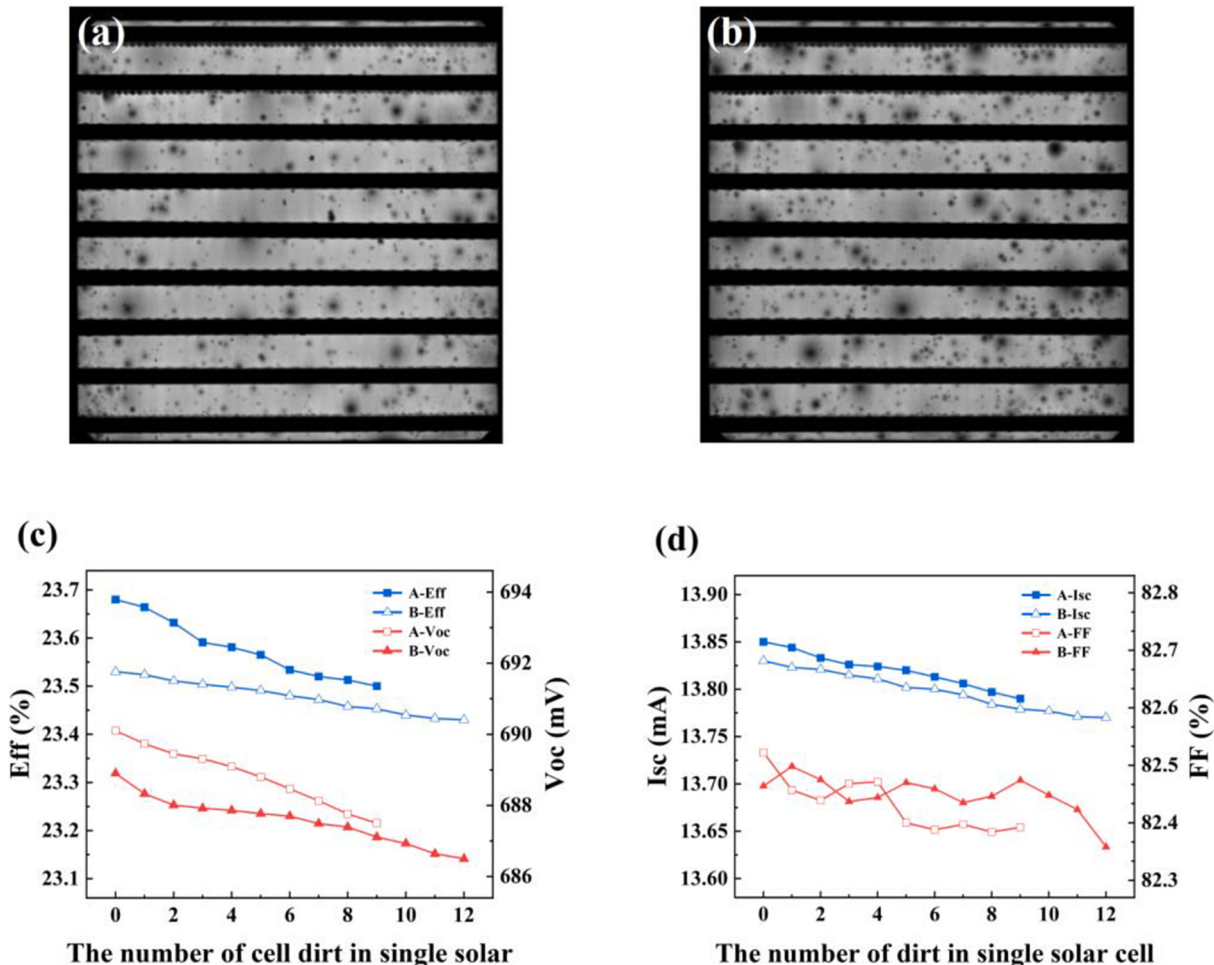


Fig. 8. (a) Electroluminescence brightness image of Group A sample; (b) Electroluminescence brightness image of Group B sample; (c) The relationship between the number of dirt and *Eff*, *Voc* in single solar cell; (d) The relationship between the number of dirt and *Isc*, *FF* in single solar cell.

in a sheet resistance of $190\ \Omega$ with a uniformity of 5.9 % and a contact resistance of $0.55\ \text{m}\Omega/\text{cm}^2$. In contrast, the conventional diffusion process yielded a sheet resistance of $168\ \Omega$ with a uniformity of 7.0 % and a contact resistance of $0.60\ \text{m}\Omega/\text{cm}^2$, as depicted in Fig. 7(a) and (b). Fig. 7(a) clearly illustrates that the high sheet resistance cells exhibit superior uniformity compared to the low sheet resistance cells. Furthermore, Fig. 7(b) emphasizes their advantageous contact resistance rates.

The Group A cells demonstrate better uniformity and contact resistance in comparison to the Group B cells, leading to reduced energy losses and improved open-circuit voltage. This, in turn, enhances photovoltaic conversion efficiency by minimizing energy dissipation and lowering the voltage drop.

The preparation of highly uniform high sheet resistance emitters not only mitigates front surface recombination and improves the open-circuit voltage but also significantly enhances the spectral response in the short wavelength range, thereby increasing the short-circuit current and overall photovoltaic conversion efficiency of the cells.

3.6. Analysis of electrical performance data

Both sets of samples were processed into finished solar cells using the conventional PERC non-SE solar cell fabrication process. However, the solar cells produced using the newly developed diffusion process demonstrated significant advantages in terms of open-circuit voltage and current, although there was a slight decrease in the fill factor. Moreover, a notable improvement in photovoltaic conversion efficiency

was observed. This improvement can be attributed to the lower surface phosphorus concentration and deeper p-n junction achieved through the diffusion process in the lightly doped region, resulting in a higher open-circuit voltage [39,40]. Additionally, the high contact resistance of the emitter region contributed to enhanced short-wavelength spectral response and carrier recombination characteristics, along with a reduction in the saturation current caused by surface recombination. Consequently, the short-circuit current was higher, as indicated in Table 4. However, it is worth noting that the uniformity of the sheet resistance from the diffusion process was slightly poorer, resulting in some losses during the filling process. If further optimization of the uniformity of the sheet resistance is achieved in subsequent stages, the photovoltaic conversion efficiency can be further improved.

As shown in Fig. S1, the EL image of a single cell can give the exact source of the dirt. However, the quality of the process needs to be analyzed from the overall EL data. Therefore, the EL images of the whole group of solar cells are synthesized. As seen in Fig. 8(a) and (b), the EL images are generated by group A and group B with ImageJ software. In other words, Fig. 8(a) and (b) are dirt combination diagrams of all the solar cells in group A and group B, respectively. By comparing Fig. 8(a) and (b), the number of dirt in group A is less than that in group B. Fig. 8(c) and Fig. 8(d) images show the relationship between the number of dirt and the IV characteristics (*Voc*, *Isc*, *FF*, and *Eff*) in single solar cell. As the number of dirt increases in group A and group B, the IV characteristics of the solar cells in group A and group B is decreasing. The *Voc*, *Isc*, and *Eff* in group A have better performances than that in group B, while the performance of *FF* is inconsistencies. That indicates *FF* is not directly

related to the situation of the dirt. As seen in **Table 4**, the changes of IV characteristics in group A and group B are similar as in **Fig. 8**. From the yield of finished solar cells in **Tables 4** and it can be seen that the yield of group A (96.50 %) is higher than that of group B (94.28 %), which can also prove the number of dirt in A is lower than that of B. The primary types of defects observed in the conventional process were noncontact dirt and boat marks, whereas the newly developed diffusion process exhibited fewer instances of dirt and no sintering defects.

4. Conclusion

In this study, the diffusion process for PERC non-selective emitter solar cells is refined. The modified diffusion protocol includes two added stages: pressure holding and extended annealing time. These additions aim to elevate the sheet resistance while enhancing the diffusion resistance and intra-wafer uniformity, ultimately augmenting the solar cell photovoltaic conversion efficiency. Employing this optimized diffusion process leads to a 0.05 % increase in the efficiency of PERC solar cells, a 1.3 mV increase in open-circuit voltage, and a 20 mA increase in short-circuit current. The peak cell efficiency attained is 23.68 %, marking a 0.16 % improvement. The primary advantages of this refined process are as follows:1) The introduction of the pressure holding step after deposition ensures a more uniform distribution of gas within the diffusion furnace, facilitating a thorough reaction during the phosphorous doping phase and enhancing the intra-wafer sheet resistance uniformity.2) Extending the annealing time enhances dopant diffusion, reduces defects, and allows for the creation of lightly doped regions with low surface phosphorous concentration and deep p-n junctions. This leads to an increased open-circuit voltage and the attainment of an excellent emitter, thereby enhancing cell efficiency.3) The high sheet resistance emitter improves the short-wavelength spectral response and carrier recombination properties, reduces the saturation current, and enhances the short-circuit current.

CRediT authorship contribution statement

Yixuan Huang: Writing – review & editing, Writing – original draft. **Longqing Jiang:** Investigation, Data curation. **Long Yan:** Methodology, Investigation. **Yang Yang:** Software, Resources. **Rulong Chen:** Writing – review & editing, Validation. **Hui Cui:** Resources, Investigation. **Geng Su:** Validation, Formal analysis. **Honggang Zhang:** Project administration, Data curation. **Baoju Yang:** Project administration, Methodology. **Juan Hong:** Supervision, Project administration, Conceptualization.

Declaration of competing interest

The authors declare that they have no known competing financial interests or personal relationships that could have appeared to influence the work reported in this paper.

Data availability

Data will be made available on request.

Acknowledgments

This work was supported by the Natural Science Foundation of China under Grants 51805466 and the Project 333 of Jiangsu Province (China) under Grants 153519050.

Appendix A. Supplementary data

Supplementary data to this article can be found online at <https://doi.org/10.1016/j.mssp.2024.108552>.

References

- [1] B. Zhou, C. Cui, S. Ma, J. Bai, H. Wang, Investigation of the P-doped lead-free glass frit based on the principle of low-temperature phosphorus diffusion for multicrystalline silicon solar cells, *Sol. Energy Mater. Sol. Cell.* (2021) 230.
- [2] J. Kim, M. Ju, Y. Kim, J. Yi, Chemical stoichiometry effect of hafnium oxide (HfO_x) for passivation layer of PERC solar cells, *Mater. Sci. Semicond. Process.* 148 (2022).
- [3] A. Ebong, I.B. Cooper, B. Rounsvaille, K. Tate, A. Rohatgi, B. Bunkenburg, J. Cathey, S. Kim, D. Ruf, High efficiency inline diffused emitter (ILDE) solar cells on mono-crystalline CZ silicon, *Progress in Photovoltaics* 18 (2010) 590–595.
- [4] F. Ye, Y. Li, X. Jia, H. Guo, X. Wang, J. Ding, N. Yuan, Z. Feng, Optimization of phosphorus dopant profile of industrial p-type mono PERC solar cells, *Sol. Energy Mater. Sol. Cell.* 190 (2019) 30–36.
- [5] R. Tong, H. Zheng, S. Ma, D. Liu, C. Xu, W. Zhang, X. Liu, Enhancement of the conversion efficiency of selective emitter PERC solar cells by post-oxidation, *Mater. Sci. Semicond. Process.* 149 (2022).
- [6] B. Pal, S. Ray, U. Gangopadhyay, P.P. Ray, Novel technique for fabrication of n-type crystalline silicon selective emitter for solar cell processing, *Mater. Res. Express* (2019) 6.
- [7] R. Tong, W. Zhang, X. Ke, D. Liu, Z. Zhang, Influence of surface structure on the performance of mono-like Si PERC solar cell, *Mater. Sci. Semicond. Process.* 126 (2021).
- [8] S. Dasgupta, Understanding Solar Cell Contacts through Simulations, 2020.
- [9] S. Kashyap, J. Madan, R. Pandey, Design and parametric optimization of ion-implanted PERC solar cells to achieve 22.8% efficiency: a process and device simulation study, *Sustain. Energy Fuels* 6 (2022) 3249–3262.
- [10] D. Zhang, L. Wang, R. Jia, K. Tao, S. Jiang, H. Ge, B. Wang, Z. Gao, X. Li, M. Li, Z. Jin, Improving the performance of PERC silicon solar cells by optimizing the surface inverted pyramid structure on large-area mono-crystalline silicon wafers, *Mater. Sci. Semicond. Process.* 138 (2022).
- [11] S. Kashyap, J. Madan, R. Pandey, R. Sharma, Process and device simulations aimed at improving the emitter region performance of silicon PERC solar cells, *J. Micromech. Microeng.* 32 (2022).
- [12] N.L. Dmitruk, O.Y. Borkovskaya, A.V. Korovin, I.B. Mamontova, V.R. Romanyuk, A.V. Sukach, Low-temperature diffused p-n junction with nano/microrelief interface for solar cell applications, *Sol. Energy Mater. Sol. Cell.* 137 (2015) 124–130.
- [13] Y. Wang, S. Lv, Z. Li, Review on incorporation of alkali elements and their effects in $\text{Cu}(\text{In},\text{Ga})\text{Se}_2$ solar cells, *J. Mater. Sci. Technol.* 96 (2022) 179–189.
- [14] D. Suh, Efficient implementation of multiple drive-in steps in thermal diffusion of phosphorus for PERC solar cells, *Curr. Appl. Phys.* 18 (2018) 178–182.
- [15] S. Chakraborty, Y. Huang, M. Wilson, A.G. Aberle, J.B. Li, Mitigating light and elevated temperature induced degradation in multicrystalline silicon wafers and PERC solar cells using phosphorus diffusion gettering, *Phys. Status Solidi A* 215 (2018).
- [16] D. Ding, Y. Zhuang, Y. Cui, Y. Zhang, Z. Li, X. Zhang, Z. Ji, D. Wang, Y. Wan, W. Shen, Application of phosphorus-doped polysilicon-based full-area passivating contact on the front textured surface of p-type silicon, *Phys. Status Solidi Rapid Res. Lett.* 15 (2021).
- [17] L. Chen, U. Romer, A. Lennon, Optimization of boron diffusion process for n-type contact passivated polysilicon solar cells, *J. Xi'an Univ. Sci. Technol.* 40 (2020) 298–303.
- [18] L. Hui, Z. Zhenfeng, W. Zhiming, Z. Mitao, T. An, Research on low pressure diffusion process of large size PERC crystalline silicon solar cells, *Sol. Energy* (2022) 41–46.
- [19] Z. Jianjun, Z. Zhimin, Z. Jinchen, J. Yingsong, L. Miao, Study on the diffusion process of SE and PERC solar cells, *Sol. Energy* (2020) 52–55.
- [20] L. Wenfeng, Z. Ziyou, H. Hailong, Z. Zhengchao, Optimization design and simulation of emitter surface of PERC solar cell, *Sol. Energy* (2019) 29–35.
- [21] M. Seri, F. Mercuri, G. Ruani, Y. Feng, M. Li, Z.-X. Xu, M. Muccini, Toward real setting applications of organic and perovskite solar cells: a comparative review, *Energy Technol.* 9 (2021).
- [22] M. Subramanian, B. Nagarajan, A. Ravichandran, V. Subhash Betageri, G. S. Thirunavukkarasu, E. Jamei, M. Seyedmahmoudian, A. Stojcevski, S. Mekhilef, V.R. Minnam Reddy, Optimization of effective doping concentration of emitter for ideal c-Si solar cell device with PC1D simulation, *Crystals* 12 (2022).
- [23] H. Huang, J. Lv, Y. Bao, R. Xuan, S. Sun, S. Sneek, S. Li, C. Modanese, H. Savin, A. Wang, J. Zhao, Data of the recombination loss mechanisms analysis on Al2O3 PERC cell using PC1D and PC2D simulations, *Data Brief* 11 (2017) 27–31.
- [24] L. Zidi, A. Mekemeche, M. Beghdad, Performance analysis on conversion efficiency of PERC solar cell by PC2D simulation, *Silicon* 11 (2019) 2479–2485.
- [25] C.C. Yang, S.Y. Chou, M.C. Chen, S.K. Lin, S.Y. Chen, S.C. Liu, K.Y. Wang, T. M. Tsai, J.W. Huang, T.C. Chang, Introducing a supercritical fluid technique to reduce passivation layer interface defects in passivated emitter rear contact cells, *Mater. Sci. Semicond. Process.* 137 (2022).
- [26] P. Padhamnath, N. Nampalli, N. Nandakumar, J.K. Buatis, M.-J. Naval, A. G. Aberle, S. Duttagupta, Optoelectrical properties of high-performance low-pressure chemical vapor deposited phosphorus-doped polysilicon layers for passivating contact solar cells, *Thin Solid Films* 699 (2020).
- [27] V. Shanmugam, A. Khanna, D.J. Perez, R.V. Tabajonda, J.M.Y. Ali, A.L.M. Ortega, I.J. Garcia, B. Lim, T. Mueller, 21% efficient screen-printed n-type silicon wafer solar cells with implanted phosphorus front surface field, *Sol. Energy Mater. Sol. Cell.* 186 (2018) 124–130.
- [28] C. Chen, P. Xue, H. Lu, J. Wang, B. Jia, Y. Li, D. Qin, Y. Lin, X. Zhan, A. Novel, Weakly N-doped cathode-modifying layer in organic solar cells, *Energy Technol.* 9 (2021).

- [29] H. Ghembaza, A. Zerga, R. Saim, M. Pasquinelli, Optimization of phosphorus emitter formation from POCl_3 diffusion for p-type silicon solar cells processing, *Silicon* 10 (2018) 377–386.
- [30] D. Suh, Efficient implementation of multiple drive-in steps in thermal diffusion of phosphorus for PERC solar cells, *Curr. Appl. Phys.* 18 (2018) 178–182.
- [31] M.K. Basher, M.J. Uddin, M.K. Hossain, M.A.R. Akand, S. Biswas, M.N.H. Mia, K. M. Shorowardi, Effect of doping profile on sheet resistance and contact resistance of monocrystalline silicon solar cells, *Mater. Res. Express* 6 (2019).
- [32] T. Kirchartz, D. Cahen, Minimum doping densities for p-n junctions, *Nat. Energy* 5 (2020) 973–975.
- [33] G. Lopez, P. Ortega, M. Colina, C. Voz, I. Martin, A. Morales-Vilches, A. Orpella, R. Alcubilla, Emitter formation using laser doping technique on n- and p-type c-Si substrates, *Appl. Surf. Sci.* 336 (2015) 182–187.
- [34] P. Wei, R. Tong, X. Liu, Y. Wei, Y. Zhang, X. Liu, J. Dai, H. Yin, D. Liu, Optimization of rear-side passivation for enhancing the performance of bifacial PERC plus solar cells, *Mater. Sci. Semicond. Process.* 170 (2024).
- [35] Q. Ni, H. Ye, Y. Shu, Q. Lin, A theoretical discussion on the internal quantum efficiencies of the epitaxial single crystal GaSb thin film cells with different p-n junctions, *Sol. Energy Mater. Sol. Cell.* 149 (2016) 88–96.
- [36] K.S. Chan, M.X. Heng, D. Ananthanarayanan, K.B. Choi, J.W. Ho, Application of non-contact quantum efficiency measurement for solar cell fabrication process insights, *Sol. Energy* 233 (2022) 494–503.
- [37] B. Talukdar, S. Buragohain, S. Kumar, V. Umakanth, N. Sarmah, S. Mahapatra, Effect of spectral response of solar cells on the module output when individual cells are shaded, *Sol. Energy* 137 (2016) 303–307.
- [38] D. Liu, M. Wright, M. Goodarzi, P.R. Wilshaw, P. Hamer, R.S. Bonilla, Observations of contact resistance in TOPCon and PERC solar cells, *Sol. Energy Mater. Sol. Cell.* (2022) 246.
- [39] H. Zhu, W. Yan, Y. Liu, D. Hu, Y. Tu, Z. Huang, X. Tan, Design investigation on 100 gm-thickness thin silicon PERC solar cells with assistance of machine learning, *Mater. Sci. Semicond. Process.* 137 (2022).
- [40] Q. Wang, W. Wu, Y. Li, L. Yuan, S. Yang, Y. Sun, S. Yang, Q. Zhang, Y. Cao, H. Qu, N. Yuan, J. Ding, Impact of boron doping on electrical performance and efficiency of n-TOPCon solar cell, *Sol. Energy* 227 (2021) 273–291.